Journal of Molecular Graphics and Modelling 44 (2013) 26–32

Contents lists available at ScienceDirect

Journal of Molecular Graphics and Modelling

journal homepage: www.elsevier.com/locate/JMGM

TDDFT studies on electronic structures, chiroptical properties and solvent effect on the CD spectra of diphosphonate-functionalized polyoxomolybdates

Yuan-Mei Sang, Li-Kai Yan*, Jian-Ping Wang, Na-Na Ma, Zhong-Min Su**

Institute of Functional Material Chemistry, Faculty of Chemistry, Northeast Normal University, Ren Min Street No. 5268, Changchun, Jilin 130024, PR China

ARTICLE INFO

Article history:
Received 6 February 2013
Received in revised form 2 May 2013
Accepted 3 May 2013
Available online 10 May 2013

Keywords:
Polyoxometalate
Charge transfer
ECD spectra
Chirality

ABSTRACT

The ultraviolet–visible and electronic circular dichroism (UV–vis/ECD) spectra of diphosphonate-functionalized asymmetric cantilever-type chiral polyoxomolybdate (POM) enantiomer R-$\{Mo_2O_5[(Mo_2O_6)NH_3CH_2CH_2CH_2C(O)(PO_3)_2]_2\}^{6-}$ (**R**) were systematically investigated using time-dependent density functional theory (TDDFT) method. From the view of molecular structure and relative energy, we inferred that there is likely a structural conversion from enantiomers **R** to S-$\{Mo_2O_5[(Mo_2O_6)NH_3CH_2CH_2CH_2C(O)(PO_3)_2]_2\}^{6-}$ (**S**) via the intermediate configuration (**IN**). The ECD spectra of the enantiomer **R** were produced over the range of 3.0–6.3 eV. The UV–vis and ECD spectra of enantiomer **R** in the gas phase and different solvents were calculated. The results reveal that the UV–vis and ECD spectra of the chiral POM in gas phase, polar solvent, or non-polar solvent are different. The calculated electron density difference maps (EDDMs) display that the POM cluster is a chiroptical chromophore in studied compound.

1. Introduction

Polyoxometalates (POMs) are a large family of polyanions clusters of the early-transition-metals in high oxidation states, most commonly V^V, Mo^{VI}, and W^{VI} [1]. POMs are a rich class of inorganic clusters and exhibit remarkable physicochemical properties. They have been applied to a variety of fields, such as medicine, chemical catalysis, optics, magnetism, biology, analytical chemistry, and materials science [2–5]. Recently, the functionalization of POMs with organic groups or organometallic complexes have drawn great attention [6]. So far a large number of POMs with the incorporation of organic groups, such as imido [7–9], alkoxy [10,11], organotin [12–14], organophosphonates [15–23], carboxylic acid [24], organosilicon [25], and organoruthenium [26], have been synthesized. Moreover, organophosphonates derivatives have attracted distinct attention, and a large number of organophosphonates derivatives of POMs have been continuously synthesized. Rosenheim and Shapiro [27] firstly studied the interaction of pyrophosphate ($P_2O_7^{4-}$) with molybdate (MoO_4^{2-}) in 1923. Afterwards, Kortz synthesized chiral Strandberg-type molybdates [15] and structurally characterized two macrocyclic dodecatungstates $[(O_3POPO_3)_4W_{12}O_{36}]^{16-}$ and $[(O_3PCH_2PO_3)_4W_{12}O_{36}]^{16-}$. Zubieta [16–19] and Calin and Sevov [20] isolated a series of organophosphonate-functionalized POMs with different size, nuclearity, and multi-dimensional framework, and demonstrated that these hybrid materials exhibit a range of magnetic properties. The dodeca, octa, and hexanuclear polyoxomolybdate wheels, which were constructed by $[O_3PCH_2PO_3]^{4-}$ and $[Mo^V_2O_4(H_2O)_6]^{2-}$ fragments, were successively reported [21–23]. These complexes possess a unique topology, which have been obtained in an acetate buffer medium. Recently, Wang and co-workers used the $[Mo_2O_4(H_2O)_6]^{2-}$ fragment and alendronic acid to obtain two cantilever-type molybdophosphates $(NH_4)_4\{V^{IV}[(Mo_2O_6)NH_3CH_2CH_2CH_2C(O)(PO_3)_2]_2\}\cdot 6H_2O$ [28] and L, D-$(NH_4)_6$-$\{Mo^V_2O_4[(Mo^{VI}_2O_6)NH_3CH_2CH_2CH_2C(O)(PO_3)_2]_2\}\cdot 6H_2O$ [29]. As a continuation of the above research, they recently reported another two asymmetric cantilever-type chiral enantiomers R-$\{Mo_2O_5[(Mo_2O_6)NH_3CH_2CH_2CH_2C(O)(PO_3)_2]_2\}^{6-}$ (**R**) and S-$\{Mo_2O_5[(Mo_2O_6)NH_3CH_2CH_2CH_2C(O)(PO_3)_2]_2\}^{6-}$ (**S**), which show an efficient catalytic activity for the oxidation of benzyl alcohol to benzaldehyde by H_2O_2 [30].

During the past few years, chirality has become a crucial issue in many fields of chemistry, material science, and biology. Chiral POMs and chiral structures containing POMs, which integrate the functionalization of chiral molecules with POMs, have attracted considerable attention. It is not only because of their intriguing

* Corresponding author. Tel.: +86 13039018900.
** Corresponding author. Tel.: +86 431 85099108.
E-mail addresses: yanlk924@nenu.edu.cn (L.-K. Yan), zmsu@nenu.edu.cn (Z.-M. Su).

1093-3263/$ – see front matter © 2013 Elsevier Inc. All rights reserved.
http://dx.doi.org/10.1016/j.jmgm.2013.05.001

Table 1
Experimental and optimized geometrical parameters for enantiomer **R**.

Bond(Å)	$Mo_1'—O_1$	$Mo_2'—O_1$	$Mo_2'—O_2$	$Mo_3'—O_2$	$C_1—O_3$	$C_1—C_2$	$C_2—C_3$	$Mo_1—O_8$	$Mo_2'—O_{10}$	$C_3—C_4$
EXP	2.031	1.799	2.020	1.864	1.451	1.513	1.520	1.703	1.723	1.503
CAL	2.014	1.873	2.015	1.903	1.439	1.538	1.536	1.749	1.758	1.529
Bond(Å)	$C_4—N$	$P—O_4$	$P—O_5$	$P—O_6$	$Mo_2'—O_4$	$Mo_3'—O_4$	$Mo_1'—O_7$	$Mo_1'—O_9$	$Mo_3'—O_{11}$	$Mo_1—O_7$
EXP	1.460	1.565	1.523	1.495	2.315	2.372	1.894	1.702	1.707	1.894
CAL	1.501	1.612	1.586	1.528	2.374	2.392	1.935	1.782	1.758	1.935
Angle(°)	$Mo_1'—O_1—Mo_2'$	$Mo_2'—O_2—Mo_3'$	$Mo_3'—O_3—C_1$	$C_1—C_2—C_3$	$C_2—C_3—C_4$	$C_3—C_4—N$	$O_4—P—O_5$	$O_4—P—O_6$	$O_5—P—O_6$	$Mo_2'—O_4—Mo_3'$
EXP	159.241	110.568	120.138	114.790	111.101	111.511	112.547	111.540	112.549	85.909
CAL	159.941	111.060	120.191	113.513	112.655	109.271	111.110	112.545	112.756	85.378

variety of architectures and topologies [31,32], but also their numerous potential applications in non-linear optics, stereoselective catalysis, and medicine. The chirality of POM can derive from chiral arrangements of POM, chiral POM framework, chiral organic side chain on POM [32]. In several research groups, many synthetic strategies have been developed to obtain chiral POM architectures, which is summarized in a recent review [32]. The following strategies are commonly used: distorting the structure, forming a vacancy, replacing with other metals, and eliminating the molecular symmetry center or plane by organic decoration [33–37]. Chiral POM is often characterized by the CD spectrum over ultraviolet–visible (UV–vis) region, which is related to the electronic excitations and named as electronic CD (ECD) spectrum. Up to now, many chiral POM derivatives have been synthesized and characterized by ECD spectra [38,9].

Although there are many reports concentrating on the experimental works of chiral POMs, theoretical studies on the ECD spectra of chiral POMs by quantum chemical calculations are few [35]. As we know that it is a costly job to calculate the ECD spectrum of chiral POM due to its complexity in geometric and electronic structures [35]. However, theoretical studies on chiral POMs are necessary and invaluable to understand the electron transition origins and the electron transition origins. Theoretical approaches are very helpful to explain the CD spectra of chiral isomers [39,40]. Theoretically reproducing and predicting the ECD spectrum are helpful for specifying the absolute molecular conformation in solution and the origins of the ECD spectrum [41–43]. Ziegler and co-workers calculated the ECD spectra of metal complexes and assigned their origins in detail [44]. Time-dependent density functional theory (TDDFT) [45] has been applied to calculate the CD spectra of chiral isomers [46,47]. Compared to *ab initio* methods, TDDFT methods greatly increase the calculation accuracy and reduce the computational cost, in particular only low-lying excitations are of concern [48].

In this paper, the ECD spectrum of enantiomer **R** was simulated to explore the main electronic transition contributions to the chiropitical properties, which is expected to provide a useful supplement to the experiment. Geometry structures and the electronic properties of the cantilever-type chiral enantiomers **R** and **S** are studied using DFT calculations. On the basis of the optimized geometries, the linear optical activity of **R** is discussed by ECD and UV–vis calculations using TDDFT methods, and the main contributions of the ECD spectra are assigned. Furthermore, the solvent effect on the ECD and UV–vis spectra of **R** is explored considering the polar and non-polar solvents and the gas phase.

2. Computational methods

All the calculations in this work were carried out using the Gaussian 09W program package [49]. The geometries of all studied compounds were fully optimized using the Becke [50] and Perdew [51] exchange correlation functional. The LANL2DZ [52,53] basis set associated with the pseudopotential was used to describe the Mo atom, whereas the basis sets of 6-31G(d) for P, C, N, O, and H atoms.

TDDFT is one of the most popular methods for the calculation of excitation properties in quantum chemistry due to its efficiency and accuracy [32,34,35,54,55]. Thus, the electronic excitation energies, oscillator strengths, and rotational strengths of the studied compounds were calculated using CAM-B3LYP combined with the effective core potential (ECP) basis set LANL2DZ in this work. Moreover, the ECD spectra in gas phase and different solvents were simulated by calculating 200 excited states. The Polarizable Continuum Model (PCM) was employed to account for the polar solvent

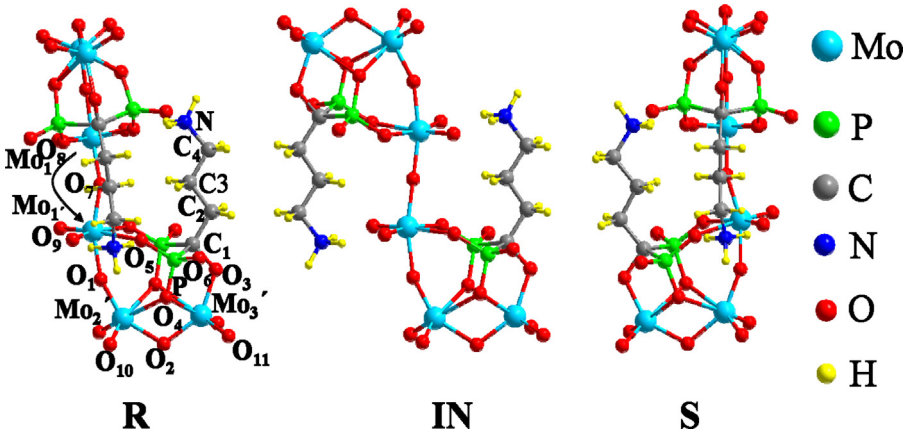

Fig. 1. Calculation models for **R**, **S** and **IN**.

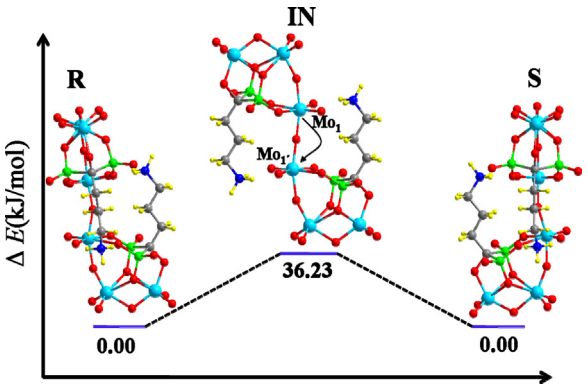

Fig. 2. Relative energy profile for **R**, **S** and **IN**.

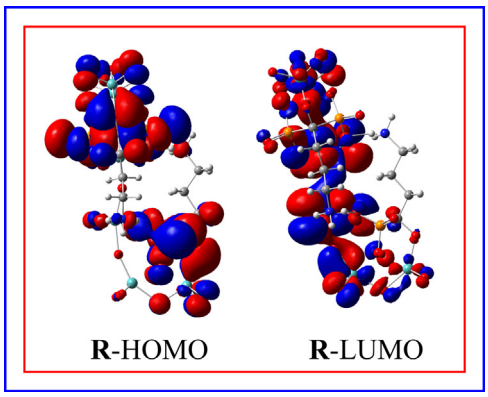

Fig. 3. Schematic orbital diagrams of **R**.

water and the non-polar solvent tetrachloromethane. Gaussian bandshape with a bandwidth of 0.2 eV was used to simulate the UV/ECD spectra.

3. Results and discussion

3.1. Geometrical and electronic structure

The two cantilever-type chiral enantiomers **R** and **S** can be described as dimeric aggregates of the $\{MoO_3[(Mo_2O_6)NH_3CH_2CH_2CH_2C(O)(PO_3)_2]\}$ unit [30]. Two $\{MoO_3[(Mo_2O_6)NH_3CH_2CH_2CH_2C(O)(PO_3)_2]\}$ fragments are connected by sharing one terminal oxygen atom of Mo_1 to form the polyanion $\{Mo_2O_5[(Mo_2O_6)NH_3CH_2CH_2CH_2C(O)(PO_3)_2]_2\}$. Some optimized and experimental geometrical parameters are listed in Table 1. Compared with experimental data, the calculated bond lengths are slightly lengthened, while bond angles are almost unchanged except the bond angle $Mo_1—O_7—Mo_{1'}$. It confirms that the computational method used here we chosen was sufficient.

Owing to the steric hindrance of alkyls, two $\{MoO_3[(Mo_2O_6)NH_3CH_2CH_2CH_2C(O)(PO_3)_2]\}$ moieties mutually rotate 90 degree resulting in enantiomers **R** and **S** with C_1 symmetry. From the structural character of enantiomers **R** and **S,** we speculated that the six molybdenum atoms of two $\{MoO_3[(Mo_2O_6)NH_3CH_2CH_2CH_2C(O)(PO_3)_2]\}$ moieties nearly locate on the same plane, which maybe exist a intermediate configuration (**IN**), and the conversion from enantiomer **R** to **S** via the intermediate **IN**. Geometrical structures of **R**, **S**, and **IN** are shown in Fig. 1. Relative energy profile for **R**, **S**, and **IN** is shown in Fig. 2. It shows that the relative energies of **R** and **S** are slightly more favorable than that of **IN** by 36.23 kJ/mol. The angle of $Mo_1—O_7—Mo_{1'}$ increases from 156.58° in **R** to 177.14° in **IN**, which the $\{MoO_3[(Mo_2O_6)NH_3CH_2CH_2CH_2C(O)(PO_3)_2]\}$ moiety has sufficient space to easily reverse. Therefore, it proposes that the conversion from enantiomer **R** to **S** via the intermediate **IN**. The possible mechanism of the structural conversion will be further studied in subsequent work.

The frontier molecular orbital (FMO) diagrams for enantiomer **R** are shown in Fig. 3. The highest occupied molecular orbital (HOMO) of **R** delocalizes over the oxygen atoms of POM and the carbon atoms of alendronic acid fragments. The lowest unoccupied molecular orbital (LUMO) of **R** predominantly localizes on six molybdenum atoms. It proposes that the studied compounds are likely to generate CT transitions in POM cluster. In enantiomer **R**, six Mo atoms not equivalent, and the abilities of six Mo atoms accepting electrons are not equal. The Mo_1 and Mo_1' have significant contributions (28%) for LUMO, while the contributions from Mo_2 and Mo_2', as well as Mo_3 and Mo_3' are less than 3%. It predicts that Mo_1 and Mo_1' atoms are easier to accept electrons in redox process.

3.2. The UV–vis and ECD spectra of the studied system

So far few theoretical works have been investigated to explore the POM-based chiral compounds [32,54–56]. The chiral enantiomers show same ECD absorptions with opposite signs and the same physicochemical properties, so only the enantiomer **R** is discussed in this work. Herein, the UV–vis and the ECD spectra of **R** are calculated at the TDDFT/CAM-B3LYP level in PCM model. To obtain reliable results, the lowest 200 excited states were calculated to simulate the ECD spectrum of **R.**

The excitation energies, oscillator strengths, and simulated UV–vis spectrum for **R** are shown in Fig. 4. It can be seen that there are an intense absorption band A at $\lambda \approx 280$ nm ($\Delta E \approx 4.43$ eV) and a weak absorption band B at $\lambda \approx 222$ nm ($\Delta E \approx 5.59$ eV). The absorption band A is mainly contributed by the excited states 38 and 44, and the high-lying band B is mainly from the excited states 156 and 163. Each of these states is composed of several electronic transitions. To clarify the origins of the UV–vis absorptions, the electron density difference maps (EDDMs) of these states were calculated using the Gauss-Sum2.2.3 software package [57]. EDDM is a representation of the changes in electron density for a given electronic transition. The calculated EDDMs together with their

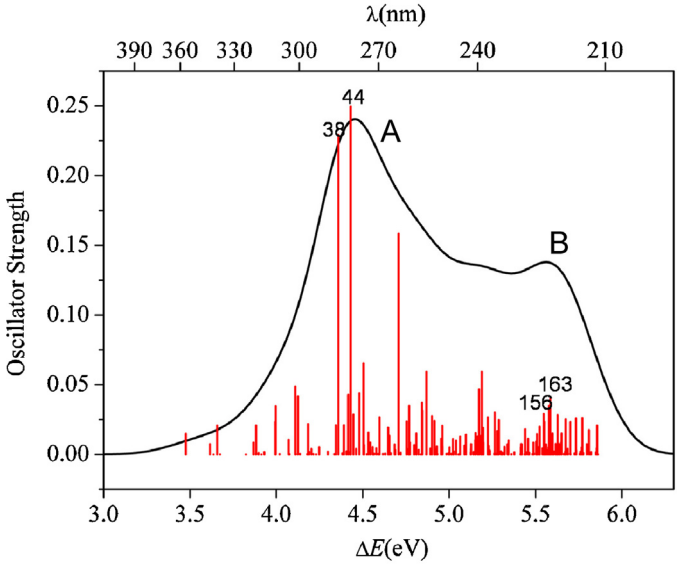

Fig. 4. The UV–vis spectra of enantiomer **R**. The half bandwidth of $\sigma = 0.2$ eV.

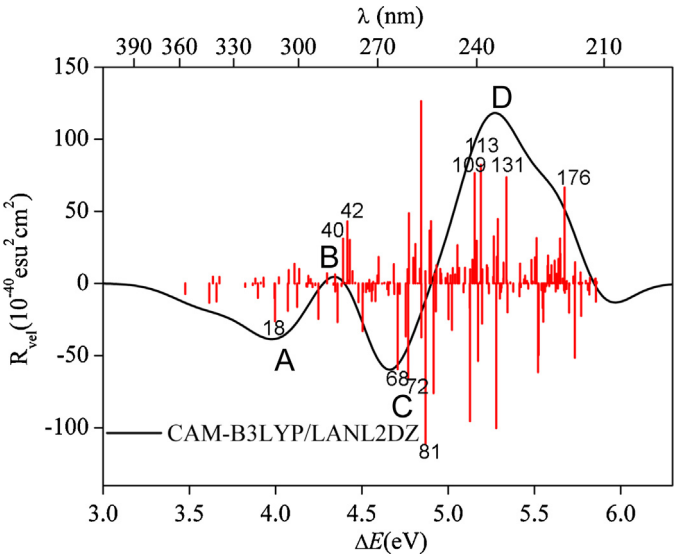

Fig. 5. The ECD spectra of enantiomer **R**. The half bandwidth of $\sigma = 0.2$ eV.

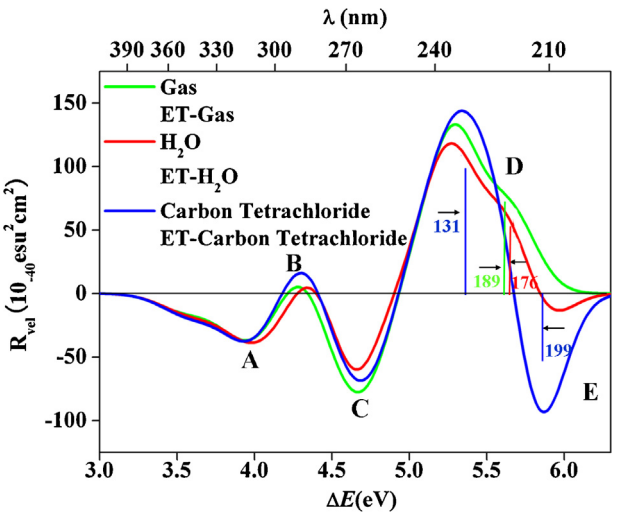

Fig. 6. The ECD spectra of chiral system enantiomer **R** in gas phase and different solvents.

corresponding transition symmetries, dominant electron transitions, and coefficients are listed in Table S1 and Fig. S1 (ESI). For enantiomer **R**, the absorption bands A and B involve the CT transitions from oxygen atoms of POM and carbon atoms of alendronic acid fragments to six molybdenum atoms (CT_1). It is found that the charge-transfer of UV–vis spectrum is consistent with the electronic distributions of FMOs.

Fig. 5 illustrates the calculated excitation energies, the corresponding optical rotatory strengths, and the simulated ECD spectrum of enantiomer **R**. There are two couplets positive Cotton effects in the ECD spectrum of **R**. The first CD couplet is at $\Delta E \approx 3.00$–4.42 eV corresponding to the rotatory absorptions of the excitations at $\Delta E \approx 4.43$ eV in UV–vis spectrum. The negative ECD band A at $\Delta E \approx 4.00$ eV is mainly from the excited state 18, and the small positive ECD band B at $\Delta E \approx 4.30$ eV is mainly from the excited states 40 and 42. While, the second CD couplet at $\Delta E \approx 4.66$–5.86 eV originates from the rotatory absorptions of the excitation at $\Delta E \approx 5.59$ eV in UV–vis spectrum. The negative ECD band C at $\Delta E \approx 4.66$ eV is mainly from the excited states 68, 72 and 81, and the broad positive ECD band D, including a positive band at $\Delta E \approx 5.34$ eV and a shoulder band at $\Delta E \approx 5.67$ eV, is mainly from the excited states 109, 113, 131, and 176. According to the EDDMs of these states, the main contribution of ECD bands for enantiomer **R** is assigned to the CT_1 (Table 2) (ESI Table S1). The results suggest that the POM is a chiroptical chromophore.

3.3. *The solvent effect on the ECD spectrum of* ***R***

The investigation of optical activity in condensed media has enjoyed a long and fruitful history [50], serving to elucidate many of the key features that distinguish the structure and dynamics of chiral molecules. However, the solvent effect on the ECD spectra of POMs compounds has not been reported. We are motivated to investigate the solvent effect on the chiropitcal properties of POMs. The selected solvent species span a wide range of chemical and physical characteristics, which can be divided into polar solvent (water) and non-polar solvent (tetrachloromethane).

Figs. 6 and 7 present the ECD and UV–vis spectra of enantiomer **R** in gas phase and different solvents. It can be seen that the Cotton bands observed in gas phase and polar solvent have similar shapes and absorption sites, while the magnitudes in polar solvent are larger than those in gas phase (Fig. 6). Compared with those in gas phase and polar solvent, the ECD spectrum of enantiomer **R** in non-polar solvent tetrachloromethane shows similar bands A, B, C, and D but the magnitudes slightly varied. It is worth noting that a new negative band E appears and mainly from the excited states 189 and 199 in the ECD spectrum of enantiomer **R** in non-polar solvent, according to EDDMs, the major contributions of excited state 189 are assigned to the CT_1 (ESI Fig. S2), while the small shoulder band on the broad positive band D in gas phase and polar solvent disappears. The shoulder band of bands D in gas phase and polar solvent (water) is mainly from the excited states 189 and 176, respectively. B and D in non-polar solvent (tetrachloromethane) is mainly from the excited state 131 (Fig. 8). According to EDDMs, the major contributions of the excited states 176 in water and 131 in non-polar solvent (ESI Fig. S2) are assigned to the CT_1, and excited state 189 in gas phase are assigned to the CT transitions from oxygen atoms to six molybdenum atoms (CT_2) (ESI Fig. S3). It indicates that both the solvent and the polarity of solvent affect the ECD spectra of chiral POMs. Fig. 7 also reveals that the UV–vis spectra are different in gas phase, polar solvent, and non-polar solvent. Although they have the same shapes and absorption sites, the intensity significantly decrease from non-polar solvent and polar solvents to gas phase. It also confirms that solvent and the polarity of solvent affect the UV–vis spectra of chiral POMs. The changes

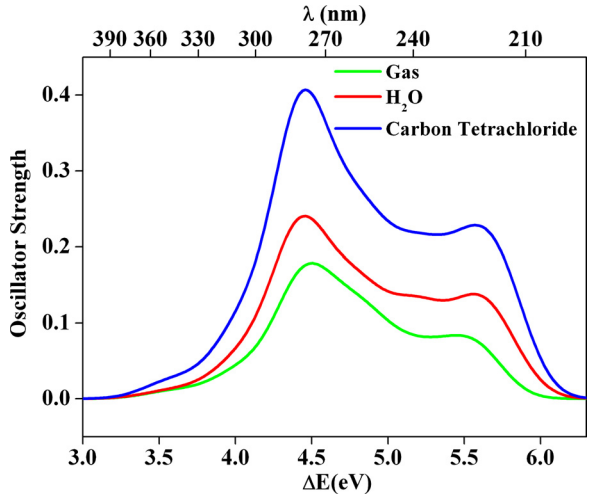

Fig. 7. The UV–vis spectra of chiral system enantiomer **R** in gas phase and different solvents.

Table 2
Excitation energies (*E*, eV), excited state, rotatory strengths, and charge transfer for ECD bands of enantiomer **R**.

Compound	Band	*E*/eV	Excited state	Rotatory strength	Charge transfer
R	A	4.00	18	−26.16	O and C atoms of alendronic acid fragments to Mo
	B	4.39, 4.42	40, 42	31.15, 43.07	O and C atoms of alendronic acid fragments to Mo
	C	4.71, 4.77	68, 72	−59.50, −66.00	O and C atoms of alendronic acid fragments to Mo
		4.87	81	−111.05	O to six Mo
	D	5.15, 5.19	109, 113	76.58, 82.26	O and C atoms of alendronic acid fragments to Mo
		5.34	131	73.67	O to six Mo
		5.67	176	66.47	O and C atoms of alendronic acid fragments to Mo

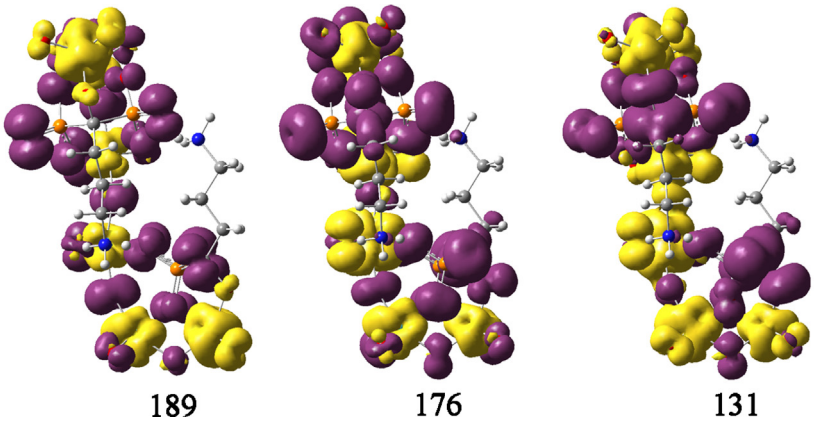

Fig. 8. The EDDMs for excited states 189, 176 and 131 of enantiomer **R** band D in gas phase and solvent phase.

in calculated spectral (CD and UV–vis) reflect the substantial influence of solvent on the optical activities of chiral POMs and shows that the solvent is an important factor to investigate chiral POMs.

4. Conclusions

In this work, we investigated the geometrical structures, electronic properties, and the solvent effect on the UV–vis and ECD spectra of the chiral diphosphonate-functionalized asymmetric cantilever-type polyoxomolybdate. TDDFT method was used to calculate the ECD spectra of chiral POM derivatives. From the view of geometrical structure, the configuration conversion form enantiomers **R** to **S** is likely via intermediate **IN**. We calculated the UV–vis and ECD spectra of enantiomer **R** in gas phase and different solvents. The results show that the UV–vis and ECD spectra of studied chiral POM have discrepancy in gas phase, polar solvent, and non-polar solvent. It discloses that the polarity of solvent influences on the chiroptical properties of studied chiral POMs. Compared with those in polar solvent and gas phase, the simulated UV–vis spectrum in non-polar solvent shows similar shapes and absorption sites, but the intensity significantly enhanced. The ECD spectra in gas phase and water have similar shapes and absorption sites, while the magnitudes in polar solvent are larger than those in gas phase. The ECD spectrum magnitudes in non-polar solvent are slightly different from those in gas phase and polar solvent. The small shoulder bands vanish and a new negative band appears in the ECD spectrum in non-polar solvent. It proposes that solvent and the polarity of solvent affect the UV–vis and the ECD spectra of chiral POMs. The main contributions of ECD bands for studied chiral POMs are ascribed to the CT transitions from oxygen atoms to six molybdenum atoms in gas phase, and the CT transitions from the oxygen atoms in POM and the carbon atoms of alendronic acid fragments to six molybdenum atoms in solvent. It suggests that the POM is a chiroptical chromophore. The presented results could be of interest in design of novel chirality controlled self-assembled systems and provide an evidence for further designing high performance optically active materials. Such systems may possess potential applications in the materials and biological sciences.

Acknowledgements

The authors gratefully acknowledge financial support by NSFC (20971020, 21073030 and 21131001), Program for New Century Excellent Talents in University (NCET-10-318), Doctoral Fund of Ministry of Education of China (20100043120007), and the Science and Technology Development Planning of Jilin Province (20100104).

Appendix A. Supplementary data

Supplementary data associated with this article can be found, in the online version, at http://dx.doi.org/10.1016/j.jmgm.2013.05.001.

References

[1] A. Dolbecq, E. Dumas, C.R. Mayer, P. Mialane, Hybrid organic–inorganic polyoxometalate compounds: from structural diversity to applications, Chemical Reviews 110 (2010) 6009–6048.
[2] R. Neumann, M. Dahan, Aruthenium-substituted polyoxometalate as an inorganic dioxygenase for activation of molecular oxygen, Nature 388 (1997) 353–355.
[3] K. Eguchi, I. Aso, N. Yamazoe, T. Seiyama, Catalytic activity of various 12-molbdophosphates for methacrolein oxidation, Chemistry Letters (1979) 1345–1346.
[4] J.T. Rhule, C.L. Hill, D.A. Judd, Polyoxometalates in medicine, Chemical Reviews 98 (1998) 327–358.
[5] M.T. Pope, A. Müller, Polyoxometalate chemistry: an old field with new dimensions in several disciplines, Angewandte Chemie International Edition 30 (1991) 34–38.
[6] P. Gouzerh, A. Proust, Main-group element, organic, and organometallic derivatives of polyoxometalates, Chemical Reviews 98 (1998) 77–112.
[7] H. Kwen, V.C. Young, E.A. Maatta, A diazoalkane derivative of a polyoxometalate: preparation and structure of $[Mo_6O_{18}(NNC(C_6H_4OCH_3)CH_3)]^{2-}$, Angewandte Chemie International Edition 38 (1999) 1145–1146.
[8] J. Hao, Y. Xia, L.-S. Wang, L. Ruhlmann, Y.-L. Zhu, Q. Li, P.-C. Yin, Y.-G. Wei, H.-Y. Guo, Unprecedented replacement of bridging oxygen atoms in

polyoxometalates with organic imido ligands, Angewandte Chemie International Edition 47 (2008) 2626–2630.
[9] J. Zhang, J. Hao, Y.-G. Wei, F.-P. Xiao, P.-C. Yin, L.-S. Wang, Nanoscale chiral rod-like molecular triads assembled from achiral polyoxometalates, Journal of the American Chemical Society 132 (2010) 14–15.
[10] C.P. Pradeep, D.-L. Long, G.N. Newton, Y.-F. Song, L. Cronin, Supramolecular metal oxides: programmed hierarchical assembly of a protein-sized 21 kDa $[(C_{16}H_{36}N)_{19}\{H_2NC(CH_2O)_3P_2V_3W_{15}O_{59}\}_4]^{5-}$ polyoxometalate assembly, Angewandte Chemie International Edition 47 (2008) 4388–4391.
[11] H.D. Zeng, G.R. Newkome, C.L. Hill, Poly(polyoxometalate) dendrimers: molecular prototypes of new catalytic materials, Angewandte Chemie International Edition 39 (2000) 1771–1774.
[12] U. Kortz, F. Hussain, M. Reicke, The ball-shaped heteropolytungstates $[\{Sn(CH_3)_2(H_2O)\}_{24}\{Sn(CH_3)_2\}_{12}(A\text{-}XW_9O_{34})_{12}]^{36-}$, Angewandte Chemie International Edition 44 (2005) 3773–3777.
[13] S. Bareyt, S. Piligkos, B. Hasenknopf, P. Gouzerh, E. Lacôte, S. Thorimbert, M. Malacria, Highly efficient peptide bond formation to functionalized Wells-Dawson-type polyoxotungstates, Angewandte Chemie International Edition 42 (2003) 3404–3406.
[14] S. Bareyt, S. Piligkos, B. Hasenknopf, P. Gouzerh, E. Lacôte, S. Thorimbert, M. Malacria, Efficient preparation of functionalized hybrid organic/inorganic Wells-Dawson-type polyoxotungstates, Journal of the American Chemical Society 127 (2005) 6788–6794.
[15] M. Carraro, A. Sartorel, G. Scorrano, C. Maccato, M.H. Dickman, U. Kortz, M. Bonchio, Chiral Strandberg-Type molybdates $[(RPO_3)_2Mo_5O_{15}]^{2-}$ as molecular gelators: self-assembled fibrillar nanostructures with enhanced optical activity, Angewandte Chemie 120 (2008) 7385–7389.
[16] R.C. Finn, R. Lam, J.E. Greedan, J. Zubieta, Solid-state coordination chemistry: structural influences of copper-phenanthroline subunits on oxovanadium organophosphonate phases. Hydrothermal synthesis and structural characterization of the two-dimensional materials $[Cu(phen)(VO)(O_3PCH_2PO_3)(H_2O)]$, $[\{Cu(phen)\}_2(V_2O_5)(O_3PCH_2CH_2PO_3)]$, and $[\{Cu(phen)\}_2(V_3O_5)(O_3PCH_2CH_2CH_2PO_3)_2(H_2O)]$ and of the three-dimensional phase $[\{Cu(phen)\}_2(V_3O_5)(O_3PCH_2PO_3)_2(H2O)]$, Inorganic Chemistry 40 (2001) 3745–3754.
[17] P.J. Hagrman, D. Hagrman, J. Zubieta, Organic–inorganic hybrid materials: from "simple" coordination polymers to organodiamine-templated molybdenum oxides, Angewandte Chemie International Edition 38 (1999) 2638–2684.
[18] R.C. Finn, R.S. Rarig Jr., J. Zubieta, Organic-inorganic hybrid materials: hydrothermal syntheses and structural characterization of bimetallic organophosphonate oxides of the type Mo/Cu/O/RPO_3^{2-}/organoimine, Inorganic Chemistry 41 (2002) 2109–2123.
[19] E. Burkholder, V. Golub, C.J. OïConnor, J. Zubieta, Solid state coordination chemistry: one-, two-, and three-dimensional materials constructed from molybdophosphonate subunits linked through binuclear copper tetra-2-pyridylpyrazine groups, Inorganic Chemistry 42 (2003) 6729–6740.
[20] N. Calin, S.C. Sevov, Novel mixed-valence heteropolyoxometalates: a molybdenum diphosphonate anion $[Mo^{V}_7Mo^{VI}O_{16}(O_3PPhPO_3H)_4]^{3-}$ and its one- and two-dimensional assemblies, Inorganic Chemistry 42 (2003) 7304–7308.
[21] C.D. Peloux, P. Mialane, A. Dolbecq, J. Marrot, F. Sécheresse, Mo^{V}/pyrophosphate polyoxometalate: an inorganic cryptate, Angewandte Chemie International Edition 41 (2002) 2808–2810.
[22] A. Dolbecq, L. Lisnard, P. Mialane, J. Marrot, M. Bénard, M.M. Rohmer, F. Sécheresse, Synthesis and characterization of octa- and hexanuclear polyoxomolybdate wheels: role of the inorganic template and of the counterion, Inorganic Chemistry 45 (2006) 5898–5910.
[23] A. Dolbecq, J.D. Compain, P. Mialane, J. Marrot, F. Sécheresse, B. Keita, L.R.B. Holzle, F. Miserque, L. Nadjo, Hexa- and dodecanuclear polyoxomolybdate cyclic compounds: application toward the facile synthesis of nanoparticles and film electrodeposition, Chemistry 15 (2009) 733–741.
[24] U. Kortz, M.G. Savelieff, F.Y.A. Ghali, L.M. Khalil, S.A. Maalouf, D.I. Sinno, Heteropolymolybdates of As^{III}, Sb^{III}, Bi^{III}, Se^{IV}, and Te^{IV} functionalized by amino acids, Angewandte Chemie International 41 (2002) 4070–4073.
[25] A. Mazeaud, Y. Dromzee, R. Thouvenot, Organic–inorganic hybrids based on polyoxometalates. 6. Syntheses, structure, and reactivity of the bis(*tert*-butylsilyl)decatungstophosphate $[(\gamma\text{-}PW_{10}O_{36})(t\text{-}BuSiOH)_2]^{3-}$, Inorganic Chemistry 39 (2000) 4735–4740.
[26] D. Laurencin, R. Villanneau, P. Herson, R. Thouvenot, Y. Jeannin, A. Proust, A new organometallic heteropolytungstate related to $[Sb_2W_{22}O_{74}(OH)_2]^{12-}$: synthesis and structural characterisation of the bis-$\{Ru(p\text{-}cymene)\}^{2+}$-containing anion $[Sb_2W_{20}O_{70}\{Ru(p\text{-}cymene)\}_2]^{10-}$, Chemical Communications (2005) 5524–5526.
[27] A. Rosenheim, M. Shapiro, Über molybdänsäure-phosphite und -pyrophosphate, sowie über die struktur der phosphorigen säure, Zeitschrift fur Anorganische und Allgemeine Chemie 129 (1923) 196–205.
[28] H.Q. Tan, W.L. Chen, D. Liu, Y.G. Li, E.B. Wang, Two new cantilever-type polyoxometalates constructed from $\{Mo_2O_4\}^{2+}$ fragments and diphosphonates, Dalton Transactions 39 (2010) 1245–1249.
[29] H.Q. Tan, W.L. Chen, D. Liu, Y.G. Li, E.B. Wang, Spontaneous resolution of a new diphosphonate-functionalized polyoxomolybdate, CrystEngComm 12 (2010) 4017–4019.
[30] H.Q. Tan, W.L. Chen, D. Liu, X.J. Feng, Y.G. Li, A.X. Yan, E.B. Wang, Two diphosphonate-functionalized asymmetric polyoxomolybdates with catalytic activity for oxidation of benzyl alcohol to benzaldehyde, Dalton Transactions 40 (2011) 8414–8418.
[31] A. Müller, F. Peters, M.T. Pope, D. Gatteschi, Polyoxometalates: very large clusters-nanoscale magnets, Chemical Reviews 98 (1998) 239–272.
[32] B. Hasenknopf, K. Micoine, E. Lacôte, S. Thorimbert, M. Malacria, R. Thouvenot, Chirality in polyoxometalate chemistry, European Journal of Inorganic Chemistry (2008) 5001–5013.
[33] L.K. Yan, X. López, J.J. Carbó, R. Sniatynsky, D.C. Duncan, J.M. Poblet, On the origin of alternating bond distortions and the emergence of chirality in polyoxometalate anions, Journal of the American Chemical Society 130 (2008) 8223–8233.
[34] Y.M. Sang, L.K. Yan, J.P. Wang, S.Z. Wen, Z.M. Su, TDDFT studies on the electronic structures and chiroptical properties of mono-tin-substituted Wells–Dawson polyoxotungstates, Journal of Physical Chemistry A 116 (2012) 4152–4158.
[35] J.P. Wang, G.C. Yang, L.K. Yan, W. Guan, S.Z. Wen, Z.M. Su, TDDFT studies on chiral organophosphonate substituted divacant Keggin-type polyoxotungstate: diplex multistep-redox-triggered chiroptical and NLO switch, Dalton Transactions 41 (2012) 10097–10104.
[36] F.-B. Xin, M.T. Pope, Lone-pair-induced chirality in polyoxotungstate structures: tin(II) derivatives of A-type $XW_9O_{34}^{n-}$ (X = P, Si). Interaction with amino acids, Journal of the American Chemical Society 118 (1996) 7731–7736.
[37] H.Q. Tan, Y.G. Li, Z.M. Zhang, C. Qin, X.L. Wang, E.B. Wang, Z.M. Su, Chiral polyoxometalate-induced enantiomerically 3D architectures: a new route for synthesis of high-dimensional chiral compounds, Journal of the American Chemical Society 129 (2007) 10066–10067.
[38] F.P. Xiao, J. Hao, J. Zhang, C.L. Lv, P.C. Yin, L.S. Wang, Y.G. Wei, Polyoxometalatocyclophanes: controlled assembly of polyoxometalate-based chiral metallamacrocycles from achiral building blocks, Journal of the American Chemical Society 132 (2010) 5956–5957.
[39] A. Moscowitz, Theoretical aspects of optical activity part one: small molecules, Advances in Chemical Physics 4 (1962) 67–112.
[40] J. Oddershede, Polarization propagator calculations, Advances in Quantum Chemistry 11 (1979) 275–352.
[41] G.C. Yang, J. Li, Y. Liu, T.L. Lowary, Y.J. Xu, Determination of the absolute configurations of bicyclo[3.1.0]hexane derivatives *via* electronic circular dichroism, optical rotation dispersion and vibrational circular dichroism spectroscopy and density functional theory calculations, Organic & Biomolecular Chemistry 8 (2010) 3777–3783.
[42] P. Mukhopadhyay, P. Wipf, D.N. Beratan, Optical signatures of molecular dissymmetry: combining theory with experiments to address stereochemical puzzles, Accounts of Chemical Research 42 (2009) 809–819.
[43] C. Bertucci, L.F.L. Guimaraes, P.S. Bonato, K.B. Borges, L.T. Okano, G. Mazzeo, C. Rosini, Assignment of the absolute configuration at the sulfur atom of thioridazine metabolites by the analysis of their chiroptical properties: the case of thioridazine 2-sulfoxide, Journal of Pharmaceutical and Biomedical Analysis 52 (2010) 796–801.
[44] J. Fan, T. Ziegler, A theoretical study on the exciton circular dichroism of propeller-like metal complexes of bipyridine and tripodal tris(2-pyridylmethyl)amine derivatives, Chirality 23 (2011) 155–166.
[45] J. Autschbach, T. Ziegler, S.J.A. van Gisbergen, E.J. Baerends, Chiroptical properties from time-dependent density functional theory. I. Circular dichroism spectra of organic molecules, Journal of Chemical Physics 116 (2002) 6930–6940.
[46] L. Rosenfeld, Quantenmechanische theorie der natürlichen optischen aktivität von flüssigkeiten und gasen, Zeitschrift fur Physiotherapie 52 (1928) 161–174.
[47] E.U. Condon, Theories of optical rotatory power, Reviews of Modern Physics 9 (1937) 432–457.
[48] R. Bauernschmitt, R. Ahlrichs, Treatment of electronic excitations within the adiabatic approximation of time dependent density functional theory, Chemical Physics Letters 256 (1996) 454–464.
[49] M.J. Frisch, G.W. Trucks, H.B. Schlegel, G.E. Scuseria, M.A. Robb, J.R. Cheeseman, G. Scalmani, V. Barone, B. Mennucci, G.A. Petersson, H. Nakatsuji, M. Caricato, X. Li, H.P. Hratchian, A.F. Izmaylov, J. Bloino, G. Zheng, J.L. Sonnenberg, M. Hada, M. Ehara, K. Toyota, R. Fukuda, J. Hasegawa, M. Ishida, T. Nakajima, Y. Honda, O. Kitao, H. Nakai, T. Vreven, J.A. Montgomery Jr., J.E. Peralta, F. Ogliaro, M. Bearpark, J.J. Heyd, E. Brothers, K.N. Kudin, V.N. Staroverov, R. Kobayashi, J. Normand, K. Raghavachari, A. Rendell, J.C. Burant, S.S. Iyengar, J. Tomasi, M. Cossi, N. Rega, J.M. Millam, M. Klene, J.E. Knox, J.B. Cross, V. Bakken, C. Adamo, J. Jaramillo, R. Gomperts, R.E. Stratmann, O. Yazyev, A.J. Austin, R. Cammi, C. Pomelli, J.W. Ochterski, R.L. Martin, K. Morokuma, V.G. Zakrzewski, G.A. Voth, P. Salvador, J.J. Dannenberg, S. Dapprich, A.D. Daniels, O. Farkas, J.B. Foresman, J.V. Ortiz, J. Cioslowski, D.J. Fox, Gaussian 09W, Revision A. 02, Gaussian, Inc., Wallingford, CT, 2009.
[50] A.D. Becke, Density-functional approximation for the correlation energy of the inhomogeneous electron gas, Physical Review A 38 (1988) 3098–3100.
[51] J.P. Perdew, Density-functional approximation for the correlation energy of the inhomogeneous electron gas, Physical Review B 33 (1986) 8822–8824.
[52] P.J. Hay, W.R. Wadt, Ab initio effective core potentials for molecular calculations. Potentials for the transition metal atoms Sc to Hg, Journal of Chemical Physics 82 (1985) 270–283.
[53] W.R. Wadt, P.J. Hay, Ab initio effective core potentials for molecular calculations. Potentials for main group elements Na to Bi, Journal of Chemical Physics 82 (1985) 284–298.
[54] J.P. Wang, L.K. Yan, W. Guan, S.Z. Wen, Z.M. Su, The structure–property relationship of chiral 1,1′-binaphthyl-based polyoxometalates: TDDFT studies on

the static first hyperpolarizabilities and the ECD spectra, Journal of Molecular Graphics and Modelling 31 (2012) 1–8.
[55] J.P. Wang, L.K. Yan, G.C. Yang, W. Guan, Z.M. Su, TDDFT studies on the structures and ECD spectra of chiral bisarylimidos bearing different lengths of o-alkoxy chain-substituted polyoxomolybdates, Journal of Molecular Graphics and Modelling 35 (2012) 49–56.
[56] S.M. Wilson, K.B. Wiberg, J.R. Cheeseman, M.J. Frisch, P.H. Vaccaro, Nonresonant optical activity of isolated organic molecules, Journal of Physical Chemistry A 109 (2005) 11752–11764.
[57] N.M. O'boyle, A.L. Tenderholt, K.M. Langner, Software news and updates cclib: a library for package-independent computational chemistry algorithms, Journal of Computational Chemistry 29 (2008) 839–845.